pH Dependence of the Flash-Induced S-State Transitions in the Oxygen-Evolving Center of Photosystem II from *Thermosynechoccocus elongatus* as Revealed by Fourier Transform Infrared Spectroscopy†

Hiroyuki Suzuki,‡ Miwa Sugiura,§ and Takumi Noguchi*,‡

Institute of Materials Science, University of Tsukuba, Tsukuba, Ibaraki 305-8573, Japan, and Department of Applied Biological Chemistry, Faculty of Agriculture, Osaka Prefecture University, 1-1 Gakuen-cho, Sakai, Osaka, 599-8531 Japan

Received August 4, 2004; Revised Manuscript Received November 9, 2004

ABSTRACT: pH dependence of the efficiencies of the flash-induced S-state transitions in the oxygen-evolving center (OEC) was studied by means of Fourier transform infrared (FTIR) difference spectroscopy using photosystem II (PSII) core complexes from the thermophilic cyanabactrium *Thermosynechoccocus elongatus*. The PSII core complexes dark-adapted at different pHs in the presence of ferricyanide as an electron acceptor were excited by four consecutive saturating laser flashes, and FTIR difference spectra induced by each flash were recorded in the region of 1800−1200 cm^{-1}. Each difference spectrum was fitted with a linear combination of standard spectra measured at pH 6.0, which represent the spectra upon individual S-state transitions, and the transition efficiencies were estimated from the fitting parameters. It was found that the $S_1 \rightarrow S_2$ transition probability is independent of pH throughout the pH region of 3.5−9.5, while the $S_2 \rightarrow S_3$, $S_3 \rightarrow S_0$, and $S_0 \rightarrow S_1$ transition probabilities decrease at acidic pH with p*K* values of 3.6 ± 0.2, 4.2 ± 0.3, and 4.7 ± 0.5, respectively. These findings, i.e., the pH-independent $S_1 \rightarrow S_2$ transition probability and the p*K* values for the inhibition in the acidic range of the other three transitions, were in good agreement with recent results obtained by electron paramagnetic resonance measurements for PSII-enriched membranes of spinach [Bernát, G., Morvaridi, F., Feyziyev, Y., and Styring, S. (2002) *Biochemistry 41,* 5830−5843]. On the basis of this correspondence for quite different types of PSII preparations exhibiting marked difference in the pH dependence of the apparent proton release pattern, it is concluded that the inhibition of the $S_2 \rightarrow S_3$, $S_3 \rightarrow S_0$, and $S_0 \rightarrow S_1$ transitions in the acidic region is an inherent property of the OEC. This feature probably reflects proton release from substrate water in these three transitions. On the other hand, all of the S-state transitions remained generally efficient up to pH 9.5 in the alkaline region, except for a slight decrease of the $S_3 \rightarrow S_0$ transition probability above pH 8 (p*K* ∼ 10). This observation partly differs from the tendency reported for spinach preparations, suggesting that a mechanism different from that in the acidic region is responsible for the transition efficiencies in the alkaline region.

The photosynthetic oxygen evolution in plants and cyanobacteria is performed in the oxygen-evolving center (OEC)[1] located on the electron-donor side of photosystem II (PSII) (*1*−*4*). Oxygen evolution takes place as a consequence of the oxidation of water, which functions as a terminal electron donor of the electron transport chain, producing NADPH and ATP for the ultimate reduction of carbon dioxide leading to the synthesis of sugars. The molecular oxygen released as a byproduct of water oxidation is basically the sole source of the oxygen content (∼21%) of the atmosphere of earth. It has been known that the catalytic site of OEC consists of a tetranuclear Mn cluster. The structure of this Mn cluster has been studied by using spectroscopic techniques such as extended X-ray absorption fine structure (EXAFS) (*3*, *5*) and electron paramagnetic resonance (EPR) (*2*, *6*). Recent results of X-ray crystallography by Zouni et al. (*7*), Kamiya and Shen (*8*), and Ferreira et al. (*9*) at resolutions of 3.8−3.5 Å led to the conclusion that the Mn cluster exhibits a trimer/monomer structure. However, these resolutions are still not sufficient to draw an unequivocal conclusion. Ferreira et al. (*9*) further proposed that carboxylate side chains from D1 (Asp170, Glu189, Glu333, and Asp342) and CP43 (Glu354) and a histidine imidazole (D1-His337) act as protein ligands to the Mn ions. The latter conclusion is consistent with mutational studies (*1*, *10*, *11*).

In contrast to the recent advancement in structural studies of the OEC, the molecular mechanism of water oxidation is

† This study was supported by a Grant-in-Aid for Scientific Research (14540607) from the Ministry of Education, Culture, Sports, Science, and Technology of Japan and by Special Research Project "Nano-Science" at the University of Tsukuba.

* To whom correspondence should be addressed. Phone: +81-29-853-5126. Fax: +81-29-855-7440. E-mail: tnoguchi@ims.tsukuba.ac.jp.

‡ University of Tsukuba.

§ Osaka Prefecture University.

[1] Abbreviations: Ches, *N*-cyclohexyl-2-aminoethanesulfonic acid; DCBQ, 2,6-dichlorobenzoquinone; DCMU, 3-(3,4-dichlorophenyl)-1,1-dimethylurea; EPR, electron paramagnetic resonance; EXAFS, extended X-ray absorption fine structure; FTIR, Fourier transform infrared; Mes, 2-(*N*-morpholino)ethanesulfonic acid; OEC, oxygen-evolving center; PSII, photosystem II; Tes, *N*-tris(hydroxymethyl)methyl-2-aminoethanesulfonic acid.

10.1021/bi0483312 CCC: $30.25
Published on Web 01/15/2005

still largely unknown. The view established so far is that two water molecules are oxidized to produce one molecular oxygen and four protons through a light-driven cycle, the so-called S-state cycle, which comprises five intermediates, the S_0−S_4 states (*12*, *13*). Among these intermediates, the S_1 state is the most dark stable, and four consecutive flashes proceed the S_1 state to S_2, S_2 to S_3, S_3 to S_0, and S_0 to the original S_1 state. Molecular oxygen is released during the $S_3 \rightarrow S_0$ transition via the transient S_4 state. As for the proton release steps, the release pattern of 1:0:1:2 for the $S_0 \rightarrow S_1 \rightarrow S_2 \rightarrow S_3 \rightarrow S_0$ transitions has long been accepted (*14*−*17*). However, it was later found that this pattern was strongly dependent on material and pH and the values were generally nonintegers *(18*, *19)*. Thus, apparent proton release upon individual S-state transitions is attributed not only to protons from substrate water but also to protons from amino acid side groups by their pK_a shifts triggered by electrostatic and conformational changes.

The redox potential (E) of the reaction of water oxidation

$$2H_2O = O_2 + 4H^+ + 4e^-$$

is pH-dependent and generally expressed as

$$E\,(\mathrm{V}) = +1.23 - 0.059\mathrm{pH} \qquad (1)$$

under conditions of the temperature of 25 °C and an O_2 pressure of 1 atm. As the pH of a medium is lowered, the redox potential increases and hence oxidation of water by P680 via Y_Z, whose redox potentials were estimated to be ∼1.2 V (*20*, *21*) and ∼1.0 V (*22*), respectively, should be inhibited. In fact, it has been observed that oxygen evolution of PSII particles or thylakoids decreases below pH 5.0 and is almost completely inhibited at pH 4.0 (*23*−*25*). For understanding the water oxidation mechanism, it is essential to examine which transitions are sensitive to pH change, because transitions including steps of proton release from substrate water should be affected by pH in principle. On the other hand, pH dependence of the S-state transitions could be affected also by protonation/deprotonation of specific amino acid groups that are involved in the mechanisms of the OEC reactions. Identification of such residues would be an important clue to understand the molecular process of water oxidation.

pH dependence of the S-state transitions has been studied by EPR (*26*, *28*), thermoluminescence (TL) (*27*), and the oscillation of oxygen yield (*29*, *30*) using thylakoids or PSII-enriched membranes of spinach. It was shown that the $S_1 \rightarrow S_2$ transition is independent of pH (*26*, *28*) and that the $S_3 \rightarrow [S_4] \rightarrow S_0$ transition is inhibited at high pH (*27*). Recently, Bernát et al. (*28*) studied the pH dependence of all four individual transitions more systematically and in a wider pH range, using the S_0, S_2, and S_3 ($S_2Y_Z^{\bullet}$) EPR signals in combination with a pH jump technique. They found that the three transitions other than $S_1 \rightarrow S_2$ are all inhibited at acidic pH, and in addition, the $S_2 \rightarrow S_3$ and $S_3 \rightarrow S_0$ transitions are inhibited at alkaline pH.

Fourier transform infrared (FTIR) spectroscopy is another powerful method to study both the structure and the reactions of OEC. Using a flash-induced difference technique, details of the structural changes, i.e., changes in chemical bonds and interactions of the proteins, Mn_4Ca core, and substrate, during the S-state cycle can be detected at the molecular level (*31*). Difference spectra upon first-, second-, third-, and fourth-flash illumination represent the changes in the $S_1 \rightarrow S_2$, $S_2 \rightarrow S_3$, $S_3 \rightarrow S_0$, and $S_0 \rightarrow S_1$ transitions, respectively (*32*−*34*). In the mid-IR region of 1800−1200 cm^{-1}, prominent signals of the amide I (1700−1600 cm^{-1}) and II (∼1550 cm^{-1}) bands because of protein conformational changes and of the carboxylate COO^- stretching bands (1600−1500 and 1450−1350 cm^{-1} for asymmetric and symmetric stretches, respectively) of Asp, Glu, and the C terminus have been observed (*35*−*43*). The presence of a number of bands of COO^- vibrations (*37*, *43*) indicates that several carboxylate groups are involved in the structure of OEC and its reactions, being consistent with the recent X-ray crystallographic structures of OEC (*8*, *9*). Chu et al. (*39*) recently identified the COO^- bands of the C terminus carboxylate in the S_2/S_1 difference spectrum, suggesting that the C terminus is strongly coupled to the Mn cluster. FTIR spectra have also been detected in the regions of the water OH stretch (3800−3000 cm^{-1}) (*44*, *45*), histidine C−N stretch (∼1100 cm^{-1}) (*46*), and Mn−O−Mn and Mn−ligand vibrations (1000−350 cm^{-1}) (*38*, *43*, *47*−*50*), providing various structural information.

Because the proton release pattern of OEC differs depending on material and pH, it is of significance to examine whether the pH dependence of the individual S-state transitions is rather similar, if not identical, in different species and preparations. If a close similarity exists, this pH dependence would reflect an intrinsic property of OEC, most likely of the proton release from substrate water itself rather than that from amino acid groups as a secondary effect of reactions. In this study, we have investigated the pH dependence of four individual S-state transitions of the OEC by means of flash-induced FTIR difference spectroscopy using the PSII core complexes from the thermophilic cyanobacterium *Thermosynchococcus elongatus*. This is a important complement to a recent study addressing the problem by using EPR spectroscopy and PSII-enriched membranes of spinach (*28*). Robustness of the core complexes of *T. elongatus* (*51*), which have been used for crystallography (*7*, *9*), enabled us to examine the pH effect on the S-state cycle in a wider pH range (pH 3.5−9.5) than before. Because individual FTIR difference spectra during the S-state cycle exhibit characteristic features with multiple peaks, the efficiencies of the four transitions could be estimated by a simple fitting procedure without any complicated experimental protocols. Furthermore, the FTIR spectroscopy has the advantage of a direct monitoring of protonation/deprotonation of amino acid groups, especially carboxylate groups, coupled to the S-state transitions, which could be relevant to the pH dependence.

MATERIALS AND METHODS

Oxygen-evolving PSII core complexes from *T. elongatus*, in which the carboxyl terminus of the CP43 subunit was genetically histidine-tagged, were purified using Ni^{2+}-affinity column chromatography as described previously (*51*). The PSII core complexes were suspended in 40 mM 2-(*N*-morpholino)ethanesulfonic acid (Mes)-NaOH buffer (pH 6.5) containing 20 mM NaCl, 15 mM $CaCl_2$, 15 mM $MgCl_2$, 15 mM imidazole, 25% glycerol, and 0.06% *n*-dodecyl β-D-maltoside and stored in liquid N_2 until use.

For FTIR measurements, the above buffer was replaced with 1 mM Mes-NaOH buffer (pH 6.0) containing 5 mM NaCl, 5 mM $CaCl_2$, and 0.06% *n*-dodecyl β-D-maltoside and then concentrated to about 4.5 mg Chl/mL using Microcon-100 (Amicon). For flash-induced measurements of the S-state cycle, the core solution (4 μL) was first mixed with 1 μL of 100 mM potassium ferricyanide solution and lightly dried on a CaF_2 plate (25 mmϕ × 3 mm) under N_2 gas flow. Then, 4 μL of 10 mM buffer at an intended pH was mixed with the sample, and the resultant solution was dried again to make a film about 1 cm in diameter on the CaF_2 plate. The dry film was moderately hydrated by humidity control using a 20% (v/v) glycerol/water solution as reported previously (*34*). Buffers used to adjust final pHs were L-glutamic acid-NaOH for pH 3.5−5.0, Mes-NaOH for pH 5.5−7.0, *N*-tris(hydroxymethyl)methyl-2-aminoethanesulfonic acid (Tes)-NaOH for pH 7.5−8.0, and *N*-cyclohexyl-2-aminoethanesulfonic acid (Ches)-NaOH for pH 8.6−10.0. The sample temperature was adjusted to 10 °C by circulating cold water in a copper holder. Flash-induced FTIR difference spectra were measured as described previously (*34*) using a Bruker IFS-66/S spectrophotometer equipped with an MCT detector (InfraRed D316/8), and a Q-switched Nd/YAG laser [Quanta-Ray GCR-130, 532 nm, ~7 ns full width at half-maximum (fwhm)]. Briefly, after two preflashes followed by subsequent dark adaptation for 1 h to oxidize Y_D and synchronize the OEC to the S_1 state, the sample was subjected to four consecutive flashes at 10-s intervals. Five single-beam spectra (10-s scans) were recorded before, between, and after the flashes. The sample was then dark-adapted for 1 h, and this cycle was repeated 8 times. Difference spectra (after minus before a flash) were calculated for individual flashes, and the spectra for the same flash number were averaged. The conditions of the 10-s interval between flashes and the 1-h dark adaptation were determined based on the relaxation time of S_2 and/or S_3 states in the order of minutes in hydrated films in the presence of ferricyanide (*34*).

Measurements of $S_2Q_A^-/S_1Q_A$ difference spectra by continuous illumination were performed with similar PSII core films in the presence of 3-(3,4-dichlorophenyl)-1,1-dimethylurea (DCMU) instead of ferricyanide. In this case, 4 μL of the core solution in 1 mM Mes buffer (pH 6.0) was first diluted with 6 μL of water, and then 0.5 μL of 1 mM DCMU/ethanol solution was mixed (final ethanol concentration was 5%). The sample was dried on a CaF_2 plate and subsequently mixed with 4 μL of 10 mM buffer at an intended pH. Hydrated films were prepared in the same manner as the samples for flash-induced measurements. Illumination was performed by continuous red light from a halogen lamp (Sigma Koki PHL-150) equipped with a red cutoff filter (Hoya-Schott R60). The light intensity was about 17 mW/cm^2 at the sample surface. After preillumination for 5 s followed by dark relaxation for 15 min, single-beam spectra (10-s scans) were recorded before and after 5-s illumination, and a light-induced difference spectrum was calculated. The measurement was repeated 8−16 times at intervals of 15 min to improve the signal-to-noise ratio.

An FTIR difference spectrum between deprotonated and protonated states of L-glutamic acid was obtained by subtraction of the spectrum of aqueous solution (250 mM) of L-glutamic acid hydrochloride from that of the solution (250 mM) of L-glutamic acid monosodium salt. All FTIR spectra were recorded with a resolution of 4 cm^{-1}.

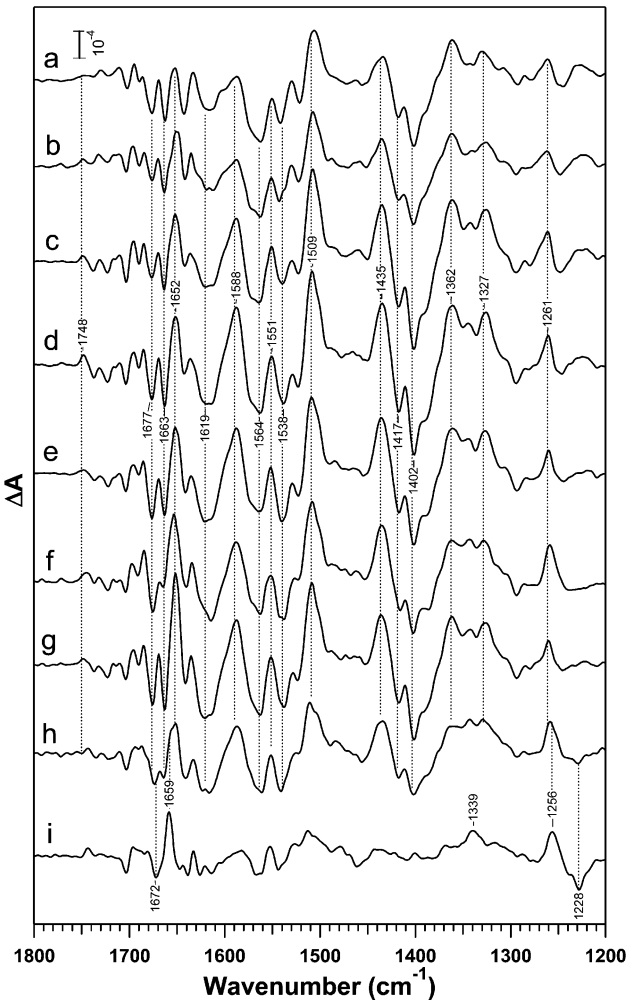

FIGURE 1: First-flash-induced FTIR difference spectra of the PSII core complexes from *T. elongatus* at pH 3.5 (a), 4.0 (b), 5.0 (c), 6.0 (d), 7.0 (e), 8.0 (f), 9.0 (g), 9.5 (h), and 10.0 (i). The core samples, in the forms of hydrated films, included ferricyanide as an electron acceptor. The sample temperature was adjusted to 10 °C. Four consecutive flashes from a Nd/YAG laser (532 nm, ~7 ns fwhm) were subjected to the sample at 10-s intervals, and an FTIR difference spectrum upon the first flash was recorded. This four-flash illumination followed by 1-h dark adaptation was repeated 8 times, and the spectra were averaged.

Spectral fitting was performed using the IGOR Pro 4.0 program (Wavemetrics Inc.).

RESULTS

Flash-induced FTIR difference spectra during the S-state cycle were measured at different pHs (pH 3.5−10.0) using the PSII core complexes from *T. elongatus* in the presence of ferricyanide as an exogenous electron acceptor. The obtained difference spectra (1800−1200 cm^{-1}) upon first-, second-, third-, and fourth-flash illumination at several selected pHs are presented in Figures 1−4, respectively. The scales of the spectra were all normalized on the basis of the protein amount estimated by the intensity of the amide II band at ~1550 cm^{-1} in original (not light-induced difference) absorption spectra (not shown). At pH 6.0, the first-, second-, third-, and fourth-flash spectra (traces d of Figures 1−4) virtually represent the structural changes upon the $S_1 \rightarrow S_2$,

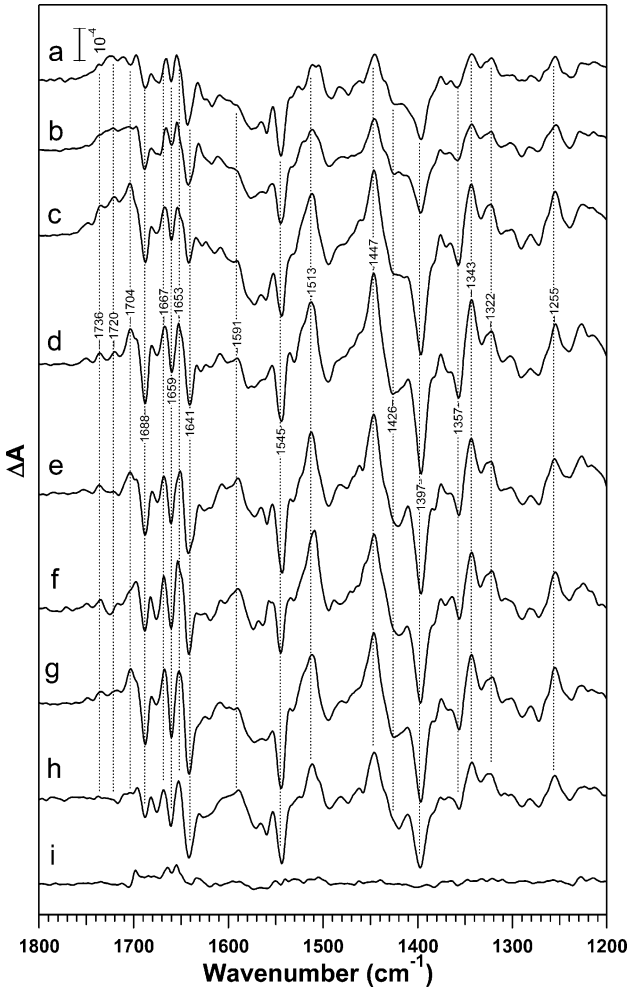

FIGURE 2: Second-flash-induced FTIR difference spectra of the PSII core complexes from *T. elongatus* at pH 3.5 (a), 4.0 (b), 5.0 (c), 6.0 (d), 7.0 (e), 8.0 (f), 9.0 (g), 9.5 (h), and 10.0 (i). Samples and measuring conditions were the same as those for Figure 1 except for recording difference spectra upon the second flash.

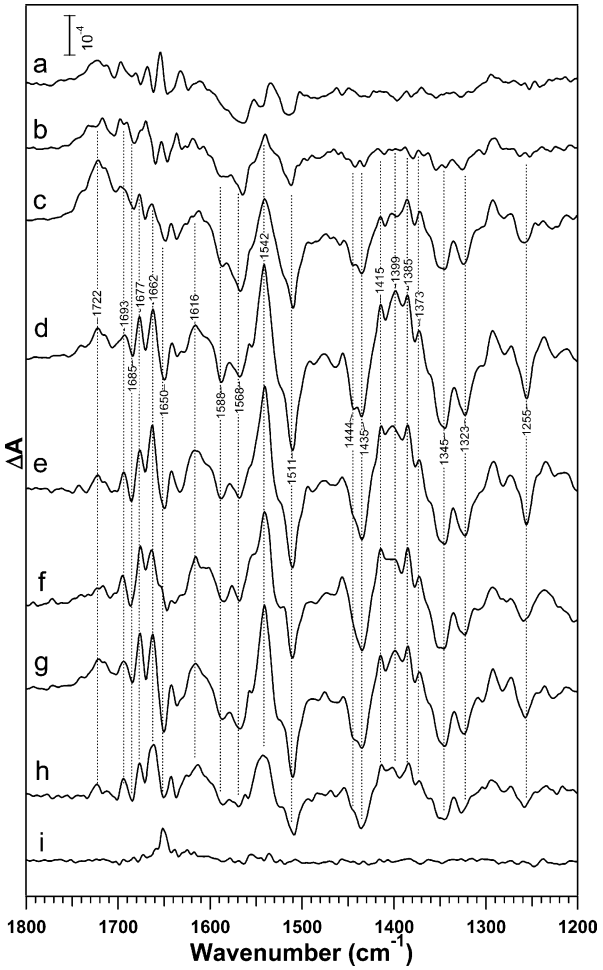

FIGURE 3: Third-flash-induced FTIR difference spectra of the PSII core complexes from *T. elongatus* at pH 3.5 (a), 4.0 (b), 5.0 (c), 6.0 (d), 7.0 (e), 8.0 (f), 9.0 (g), 9.5 (h), and 10.0 (i). Samples and measuring conditions were the same as those for Figure 1 except for recording difference spectra upon the third flash.

$S_2 \rightarrow S_3$, $S_3 \rightarrow S_0$, and $S_0 \rightarrow S_1$ transitions (*34*). The frequency region of 1800−1200 cm^{-1} comprises the protein bands that are coupled to the S-state transitions (*37*). Typically, complex structures at 1700−1600 cm^{-1} mostly arise from the amide I bands (C═O stretch) of backbones because of protein conformational changes, and prominent bands at 1450−1300 cm^{-1} originate from the symmetric COO^- stretching bands of carboxylate groups. In addition, prominent bands at 1600−1500 cm^{-1} are attributed to either the asymmetric COO^- stretching bands of carboxylate or the amide II bands (NH deformation coupled with C−N stretch) of backbones.

At the first flash (Figure 1), only the $S_1 \rightarrow S_2$ transition takes place in OEC, because a double hit does not occur by a single pulse with a ∼7 ns width. The spectral intensity gently decreased as the pH is either lowered from 6.0 to 3.5 or increased from 6.0 to 9.5. At pH 10.0 (trace i of Figure 1), however, the S_2/S_1 signals disappeared in the spectrum and instead typical signals of the non-heme iron (Fe^{2+}/Fe^{3+}) (*52*, *53*) appeared at 1672, 1659, 1339, 1256, and 1228 cm^{-1}. At this high pH, the second-, third-, and fourth-flash spectra did not show any signals (traces i of Figures 2−4). Thus, it is assumed that the OEC is totally inactivated at pH 10.0, whereas the sample includes the PSII complexes with OEC that retains its integrity between pH 3.5−9.5. At pH 9.5, although most of the signals originate from the S_2/S_1 difference, there seems to be some contributions from the non-heme iron signals (trace h of Figure 1).

At the second flash (Figure 2), signals basically identical to those in the standard S_3/S_2 spectra at pH 6.0 (trace d) were observed between pH 3.5 and 9.5. Similar to the first-flash spectra (Figure 1), the overall intensities decreased on both the acidic and alkaline sides, although this tendency seems more significant on the acidic side. A broad positive background around 1720 cm^{-1}, concomitant with negative ones around 1550 and 1400 cm^{-1}, were pronounced at pH 3.5−5.0 (traces a−c of Figure 2), the pH region in which glutamic acid is used as a buffer component. Similar broad backgrounds were seen also in the third- and fourth-flash spectra at pH 3.5−5.0 (traces a−c of Figures 3 and 4). The feature of these signals is typical of the protonation of carboxylate groups, which is characterized by the appearance of the C═O stretch of COOH at 1750−1700 cm^{-1} and the disappearance of the asymmetric and symmetric COO^- stretches at ∼1550 and ∼1400 cm^{-1}, respectively. The broad features indicate that the signals are not attributed to specific carboxylate groups inside the proteins but to glutamate buffer or nonspecific carboxylate groups on the surface of the proteins. Although the latter assignment was previously made

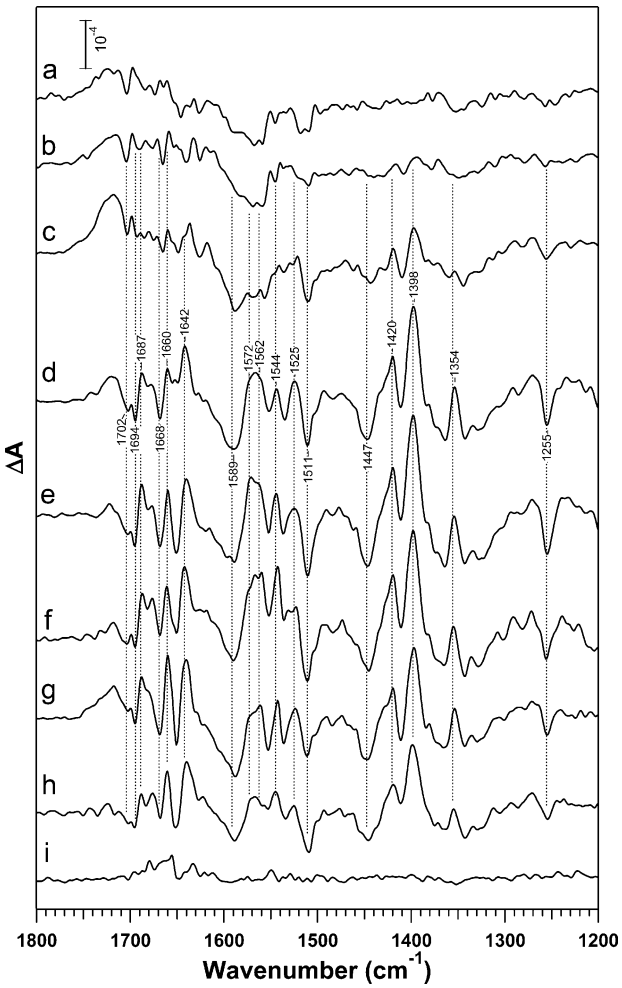

FIGURE 4: Fourth-flash-induced FTIR difference spectra of the PSII core complexes from *T. elongatus* at pH 3.5 (a), 4.0 (b), 5.0 (c), 6.0 (d), 7.0 (e), 8.0 (f), 9.0 (g), 9.5 (h), and 10.0 (i). Samples and measuring conditions were the same as those for Figure 1 except for recording difference spectra upon the fourth flash.

for similar broad features observed in the S-state spectra in solution samples (*33*), such broad features were not pronounced in samples of hydrated films at pH 6.0 (*34*) (trace d of Figure 2). Thus, it is most likely that protonation of glutamate buffer during the S-state cycle makes a major contribution to the broad features at pH 3.5−5.0.

The third- and fourth-flash spectra (Figures 3 and 4, respectively) showed basically a similar tendency of pH dependence in the region of pH 3.5−9.5. The band intensities diminished at acidic and alkaline pH values conserving basic spectral features of the S_0/S_3 (for third flash) or S_1/S_0 (for fourth flash) signals at pH 6.0. However, compared with the first- and second-flash spectra, the signal decrease by lowering pH was more significant and no prominent signals were observed at pH 3.5.

It is noteworthy that throughout the first−fourth-flash spectra, basically all of the prominent peaks of the standard spectra at pH 6.0 were conserved in the pH range of 3.5−9.5 as long as band intensities are retained (Figures 1−4). In addition, no specific peaks were newly observed by lowering or increasing pH except for broad backgrounds by protonation of buffer or nonspecific carboxylate.

To estimate the efficiencies of individual S-state transitions from these FTIR data, fitting of the spectra at each pH with the standard spectra at pH 6.0 was performed with a similar method described previously (*34*). This fitting was performed for the spectra in the symmetric COO^- region (1470−1300 cm^{-1}), because bands in this region, in contrast to the amide I (1700−1600 cm^{-1}) and II (1600−1500 cm^{-1}) regions, are not particularly sensitive to subtle changes in sample conditions such as a hydration extent and hence provide better fitting results. Before fitting the spectra, broad backgrounds mostly because of glutamate buffer in the second−fourth-flash spectra at pH 3.5−5.0 (trances a−c of Figures 2−4) were eliminated by subtracting the glutamic acid/glutamate difference spectrum obtained in aqueous solutions so as to cancel the broad positive feature around 1720 cm^{-1}. An experimentally obtained *n*th-flash spectrum at a certain pH, $f_n(\nu)$ ($n = 1-4$), was fitted with a linear combination of the standard first-, second-, third-, and fourth-flash spectra at pH 6.0 (traces d of Figures 1−4), $F_1(\nu)$, $F_2(\nu)$, $F_3(\nu)$, and $F_4(\nu)$, which virtually represent the difference spectra upon $S_1 \rightarrow S_2$, $S_2 \rightarrow S_3$, $S_3 \rightarrow S_0$, and $S_0 \rightarrow S_1$ transitions, respectively;

$$f_n(\nu) = c_{n1}F_1(\nu) + c_{n2}F_2(\nu) + c_{n3}F_3(\nu) + c_{n4}F_4(\nu) \quad (2)$$

where c_{n1}, c_{n2}, c_{n3}, and c_{n4} are the coefficients of the linear combination. In the fitting, the parameters, $c_{n1}-c_{n4}$, were restricted as follows. At the first flash ($n = 1$), c_{12}, c_{13}, and c_{14} were set to 0, because of no double hit. At the second flash ($n = 2$), c_{23} and c_{24} were set to 0 for the same reason and c_{21} was restricted to $0 < c_{21} < c_{11}$. At the third flash ($n = 3$), c_{34} was set to 0 and c_{31} and c_{32} were set to $0 < c_{31} < c_{21}$ and $0 < c_{32} < c_{22}$, respectively. Finally, at the fourth flash ($n = 4$), c_{41}, c_{42}, and c_{43} were restricted to $0 < c_{41} < c_{31}$, $0 < c_{42} < c_{32}$, and $0 < c_{43} < c_{33}$, respectively. The results of fitting are presented in Figure 5 at selected pHs of 4.0 (A), 5.0 (B), 7.0 (C), and 8.0 (D), showing that the spectra at each pH were satisfactorily fitted using the above procedure.

The efficiencies of the $S_1 \rightarrow S_2$, $S_2 \rightarrow S_3$, $S_3 \rightarrow S_0$, and $S_0 \rightarrow S_1$ transitions, $\phi_{1\rightarrow2}$, $\phi_{2\rightarrow3}$, $\phi_{3\rightarrow0}$, and $\phi_{0\rightarrow1}$, respectively, can be estimated from the quantities of the most advanced transitions at individual flashes, i.e., the fitting parameters, c_{11}, c_{22}, c_{33}, and c_{44} (*34*);

$$\begin{aligned} \phi_{1\rightarrow2} &= (1-\alpha)c_{11}/\rho_{act} \\ \phi_{2\rightarrow3} &= (1-\alpha)c_{22}/c_{11} \\ \phi_{3\rightarrow0} &= (1-\alpha)c_{33}/c_{22} \\ \phi_{0\rightarrow1} &= (1-\alpha)c_{44}/c_{33} \end{aligned} \quad (3)$$

where ρ_{act} is the number of active OEC at each pH with respect to that at pH 6.0 (see below) and α is a miss factor at pH 6.0, which was previously estimated to be 0.12 for an identical hydrated film (*34*). This miss factor is virtually identical to that of *T. elongatus* thylakoids in solution obtained by Isgandarova et al. (*54*) from the flash-induced oxygen evolution patterns measured at 10 °C. It should be noted that this procedure to estimate the transition efficiencies gives the same results as a method that pure S_2/S_1, S_3/S_2, S_0/S_3, and S_1/S_0 difference spectra are first calculated using the experimental flash spectra at pH 6.0, $F_n(\nu)$ ($n = 1-4$),

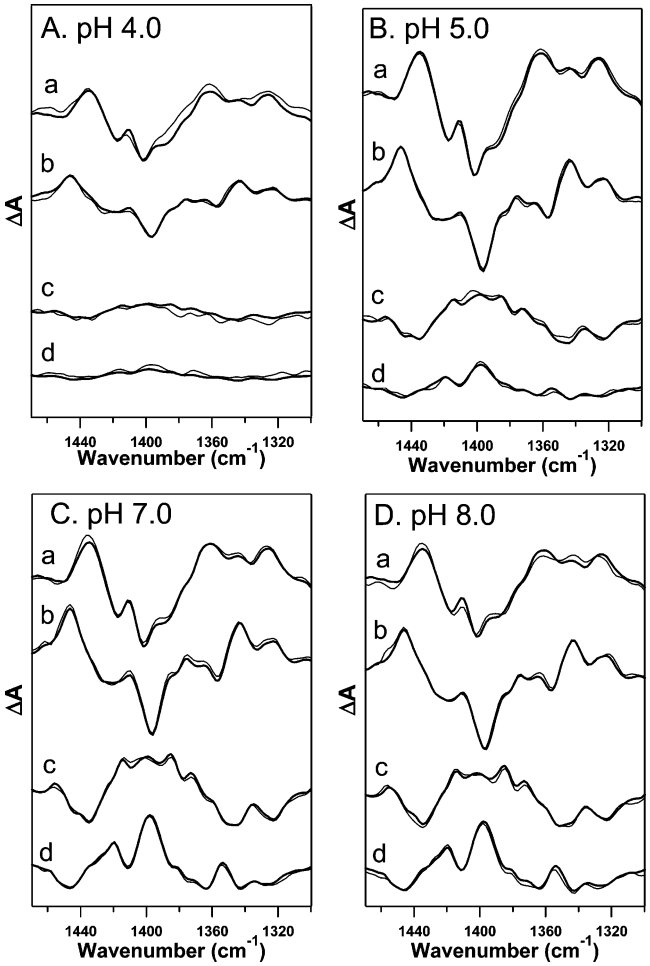

FIGURE 5: Results of fitting of the flash-induced spectra of OEC in the symmetric COO^- stretching region (1470−1300 cm^{-1}) at pH 4.0 (A), 5.0 (B), 7.0 (C), and 8.0 (D). The experimentally obtained difference spectra (thin lines) upon first (a), second (b), third (c), and fourth (d) flashes at each pH were fitted with a linear combination of four standard difference spectra (first−fourth-flash spectra) at pH 6.0. The resulting fitting spectra (thick lines) are presented in comparison with the experimental spectra. For the second-, third-, and fourth-flash spectra at pH 4.0 and 5.0 (traces b−d of A and B), the contribution of buffer (glutamic acid) changes were eliminated before fitting. See the text for details of the fitting procedure.

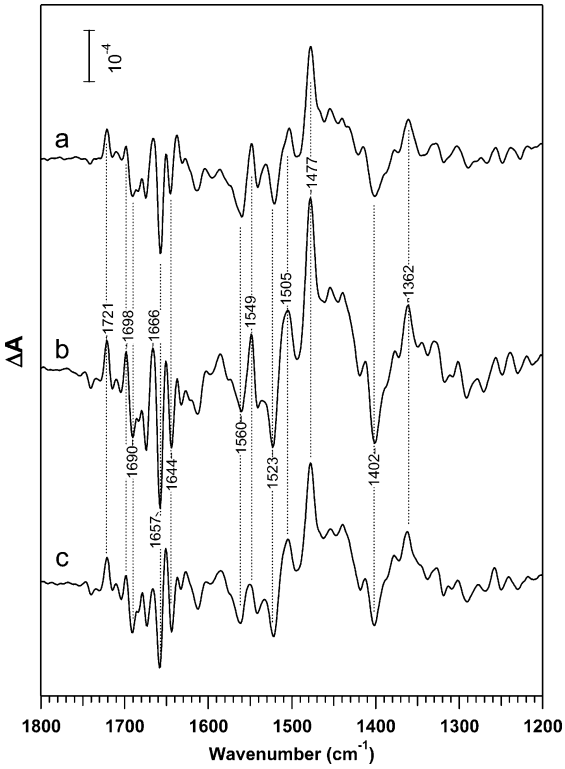

FIGURE 6: $S_2Q_A^-/S_1Q_A$ difference spectra of PSII core complexes at pH 4.0 (a), 6.0 (b), and 8.0 (c) by continuous-light illumination. The core samples included DCMU to block electron transfer beyond Q_A^-, and the sample temperature was 10 °C. Illumination was performed by continuous red light (>600 nm) for 5 s, and difference spectra between before and after illumination were recorded. The measurement was repeated at intervals of 15 min, and the spectra were averaged.

and a miss factor of 0.12, and then the spectra at each pH are fitted by these pure spectra. In this case, the efficiencies of individual transitions are obtained by the expression similar to eq 3 without the coefficient of $(1 - \alpha)$.

The value of ρ_{act} was estimated by detecting the $S_2Q_A^-$ formation by continuous illumination in the presence of DCMU. DCMU blocks an electron transfer beyond Q_A, and hence continuous illumination converts all of the active centers to the $S_2Q_A^-$ state. Thus, the intensity of the $S_2Q_A^-/S_2Q_A$ difference spectra upon this continuous illumination reflects the number of active centers. Note that because the core complexes of *T. elongatus* showed a TL band by $S_2Q_A^-$ recombination at ∼20 °C (*51*), the $S_2Q_A^-$ state is stable enough during the scan time (10 s) at the measurement temperature of 10 °C. The obtained $S_2Q_A^-/S_2Q_A$ difference spectra are presented in Figure 6 for pH 4.0 (a), 6.0 (b), and 8.0 (c). The intensities of these spectra were normalized on the basis of the protein amount estimated by the amide II band intensity in the similar way to the flash-induced spectra. These spectra showed basically the same band features irrespective of pH and were identical to the $S_2Q_A^-/S_1Q_A$ spectra previously measured for the PSII core complexes from *T. elongatus* (*55*). The characteristic positive peak at 1477 cm^{-1} has been attributed to the CO stretching vibration of a semiquinone anion (*56*, *57*), and the negative peak at 1402 cm^{-1} belongs to the S_1 state in the S_2/S_1 difference (*55*, *58*−*60*). The sum of the absolute intensities of the 1477 and 1402 cm^{-1} peaks was used to estimate the relative amount of $S_2Q_A^-$ formation, i.e., that of active OEC centers, ρ_{act}. The obtained values of ρ_{act} were plotted as a function of pH in Figure 7A (○). There is a tendency that the number of active centers decreases as the pH is decreased and increased from pH 6.0. This active-center decrease may simply originate from inactivation of OEC or PSII at low and high pHs, because prolonged incubation of the core sample in buffer solution at very high and low pHs promoted the S_2-formation loss. The decrease in the number of functionally competent OEC at acidic and/or alkaline pHs has been reported previously (*27*−*29*).

The pH dependence of the relative amount of S_2 formation by single-flash illumination, which was estimated by a fitting parameter c_{11}, is also presented in the same panel (Figure 7A, ●). It is readily seen that flash-induced S_2 formation exhibited the pH dependency similar to ρ_{act}, i.e., the smaller value at lower and higher pHs than pH 6.0. The efficiency of the $S_1 \rightarrow S_2$ transition in active centers, $\phi_{1\rightarrow2}$, estimated from eq 2 was plotted in Figure 7B as a function of pH. The data points were rather scattered probably because of

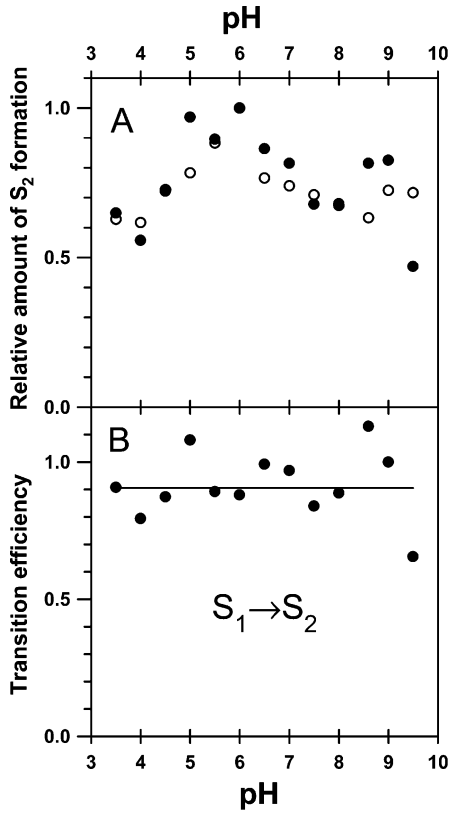

FIGURE 7: (A) Relative amount of flash-induced (●) and continuous light-induced (○) S_2 formation as a function of pH. The amount of flash-induced S_2 formation was estimated by fitting of the first-flash induced spectra at each pH with the standard S_2/S_1 difference spectrum at pH 6.0 in the 1470−1300 cm^{-1} region (Figure 1). The relative amount of continuous-light-induced S_2 formation, which represents the relative number of active OEC (ρ_{act}), was estimated from the sum of the absolute intensities of a positive 1477 cm^{-1} band (Q_A^-) and a negative 1402 cm^{-1} band (S_1) in the $S_2Q_A^-/S_1Q_A$ spectra (Figure 6). (B) pH dependence of the efficiency of the $S_1 \rightarrow S_2$ transition ($\phi_{1\rightarrow2}$). The efficiency at each pH was estimated as a ratio of the amount of flash-induced S_2 formation (A, ●) to that of continuous-light-induced S_2 formation (A, ○), multiplied by a factor of 0.88, which is an $S_1 \rightarrow S_2$ efficiency at pH 6.0 (*34*).

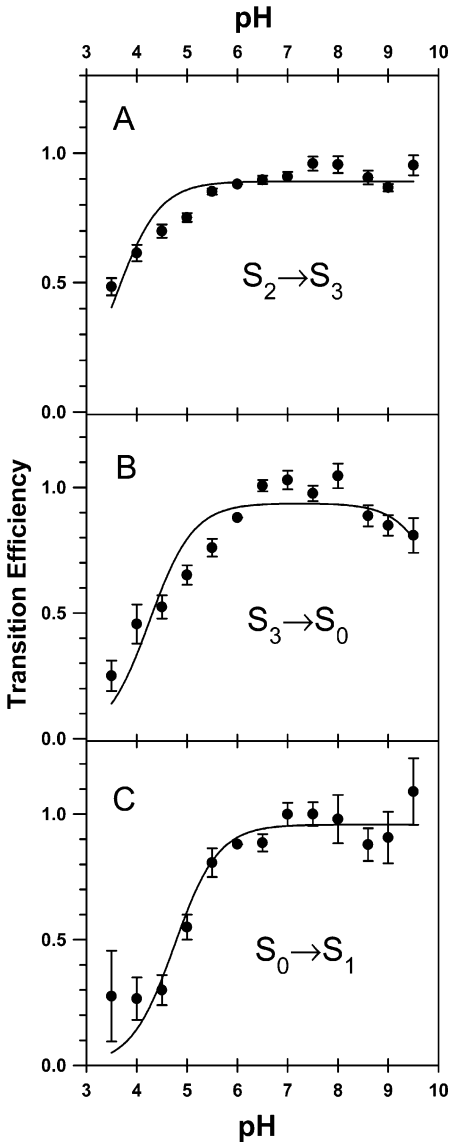

FIGURE 8: pH dependence of the efficiencies of the $S_2 \rightarrow S_3$ (A), $S_3 \rightarrow S_0$ (B), and $S_0 \rightarrow S_1$ (C) transitions estimated by fitting of the flash-induced FTIR spectra at each pH (Figures 2−4) by a linear combination of the standard difference spectra at pH 6.0 (see the text for details). Error bars were estimated from the standard deviations of the fitting parameters. Solid lines are the titration curves with one or two p*K* values to fit the data points.

relatively rough estimation of the protein amount using the amide II band. Despite the scatter, however, this plot clearly shows that the $S_1 \rightarrow S_2$ transition is pH-independent in the range of pH 3.5−9.5. This result of pH independency of the $S_1 \rightarrow S_2$ transition is in agreement with the previous studies by EPR measurements (*26*, *28*).

The efficiencies of the $S_2 \rightarrow S_3$ ($\phi_{2\rightarrow3}$), $S_3 \rightarrow S_0$ ($\phi_{3\rightarrow0}$), and $S_0 \rightarrow S_1$ ($\phi_{0\rightarrow1}$) transitions, which were estimated from the resulting fitting parameters using eq 2, were plotted in Figure 8 as functions of pH. Errors of the efficiency values were estimated from the standard deviation of the fitting parameters. In the low pH region, all of these three transitions showed an efficiency decrease. Among them, inhibition of the $S_3 \rightarrow S_0$ and $S_0 \rightarrow S_1$ transitions was more prominent than that of the $S_2 \rightarrow S_3$ transition. Titration curves to fit the data points in the acidic region provided p*K* values of 3.6 ± 0.2, 4.2 ± 0.3, and 4.7 ± 0.5 for the $S_2 \rightarrow S_3$, $S_3 \rightarrow S_0$, and $S_0 \rightarrow S_1$ transitions, respectively. It should be noted that these fitting curves assume a single-proton reaction. Actually more than one proton should be related in some transitions, and hence the deviation from the fitting curve could reflect a multiple-proton reaction. It could be possible, however, that this deviation simply arises from experimental uncertainty. Further careful studies are necessary to address this point.

In the present FTIR measurements, a constant pH was used throughout the S-state cycle. Hence, if the reaction was completely blocked at earlier transitions, it would be difficult to estimate the efficiencies of the later transitions. In such a case, we would need a kind of pH jump technique as Bernát et al. (*28*) successfully used in their EPR study, in which the pH was rapidly changed by mixing stronger buffer just before a flash for the target transition is given. However, such a situation actually took place only in the $S_0 \rightarrow S_1$ transition at pH 3.5 as shown in the very small signals at the third and fourth flashes (traces a of Figures 3 and 4) and a relatively large error bar in the calculated efficiency (Figure 8C, the point at pH 3.5). Note that omitting this point at pH 3.5 from Figure 8C changes the p*K* value for the $S_0 \rightarrow S_1$ transition only by +0.05, which is much smaller than the estimated error (±0.5). As long as transitions are advanced

Table 1: pH Dependence of the Individual S-State Transitions

	T. elongatus PSII core[a]		spinach PSII-enriched membranes[b]	
transitions	pK_1	pK_2	pK_1	pK_2
$S_1 \rightarrow S_2$	pH independent (pH 3.5−9.5)		pH independent (pH 4.1−8.4)	
$S_2 \rightarrow S_3$	3.6 ± 0.2	pH independent (pH ≤ 9.5)	4.0	9.4
$S_3 \rightarrow S_0$	4.2 ± 0.3	(10.2 ± 1.0)[c]	4.5	8.0
$S_0 \rightarrow S_1$	4.7 ± 0.5	pH independent (pH ≤ 9.5)	4.7	pH independent (pH ≤ 8.9)

[a] This study by means of FTIR difference spectroscopy. [b] Study by Bernát et al. (*28*) by means of EPR spectroscopy. [c] This value was estimated by fitting of the data to pH 9.5. The OEC was actually inactive at pH 10.0. See the text for details.

even with low probabilities, transition efficiencies can be estimated by the above method of fitting the flash-induced FTIR spectra, and thus the obtained p*K* values, which exhibited higher values for later transitions, are not an artifact by inhibition of earlier transitions. This will be verified later in comparing with the p*K*s obtained by Bernát et al. (*28*) using the pH jump technique (see below).

In contrast to the clear acidic inhibition, in the high pH region, the $S_2 \rightarrow S_3$ and $S_0 \rightarrow S_1$ efficiencies were basically independent of pH to 9.5, while the $S_3 \rightarrow S_0$ efficiency slightly decreased at pH values higher than 8.0. From a titration curve to fit this decrease, the p*K* for the alkaline inhibition of the $S_3 \rightarrow S_0$ transition was estimated to be 10.2 ± 1.0.

The overall efficiency of the S-state cycle multiplied by the active center ratio, $\rho_{act}\phi_{1\rightarrow2}\phi_{2\rightarrow3}\phi_{3\rightarrow0}\phi_{0\rightarrow1}$, should be directly related to the O_2-evolving activity by continuous illumination. The pH dependence of the above expression provided a bell-shape function with a maximum at pH ∼7 and a steeper slope on the acidic side (not shown). This overall shape was basically similar to the pH dependence of the O_2-evolving activity of the PSII cores from *T. elongatus* measured using 2,6-dichlorobenzoquinone (DCBQ) as an exogenous electron acceptor. However, O_2 evolution as a function of pH was actually highly dependent on the species of electron acceptor and light intensity. This indicates that the pH dependence of the O_2 evolution by continuous illumination reflects not only the efficiency of the S-state cycle but also the rates of the acceptor-side reactions.

DISCUSSION

We have examined pH dependence of the individual S-state transitions during oxygen evolution by means of flash-induced FTIR measurements using the core complexes of the cyanobacterium *T. elongatus*. Table 1 collects the obtained results in comparison with the results by Bernát et al. (*28*) for the PSII-enriched membranes of spinach by EPR measurements. The $S_1 \rightarrow S_2$ transition was independent of pH in the range of pH 3.5−9.5 (Figure 7B), although the number of active OEC decreased in more acidic and alkaline pH values. This result of pH independency agrees with that of the study by Bernát et al. (*28*) (pH 4.1−8.4) (Table 1) and of an early EPR study by Damoder and Dismukes (*26*) (pH 5.5−8.5). All of the other three transitions, $S_2 \rightarrow S_3$, $S_3 \rightarrow S_0$, and $S_0 \rightarrow S_1$, were inhibited by lowering pH (Figure 8 and Table 1). The p*K* values of the acidic inhibition were estimated to be 3.6 ± 0.2, 4.2 ± 0.3, and 4.7 ± 0.5 for the $S_2 \rightarrow S_3$, $S_3 \rightarrow S_0$, and $S_0 \rightarrow S_1$ transitions, respectively, which are also in good agreement with the values of spinach PSII membranes: 4.0, 4.5 and 4.7, respectively (Table 1). This excellent agreement of the pH dependence with that of the previous study by Bernát et al. (*28*) is somewhat surprising, because the two studies used totally different species, materials, and spectroscopic methods: (i) a thermophilic cyanobacterium versus a higher plant, (ii) PSII core complexes versus PSII-enriched membranes, (iii) ferricyanide versus phenyl-*p*-benzoquinone as an exogenous electron acceptor and the absence versus presence of methanol, (iv) hydrated films versus concentrated solutions, (v) same buffer throughout the S-state cycle versus a pH jump in some measurements and flash illumination at 10 °C versus 20 °C, and (vi) FTIR versus EPR spectroscopy. The good agreement despite these different conditions, therefore, indicates that the obtained results are highly reliable. Thus, the pH independence of the $S_1 \rightarrow S_2$ transition and the acid inhibition in the other three transitions are probably inherent properties of OEC irrespective of species and preparations.

Possible factors responsible for the acidic inhibition in the $S_2 \rightarrow S_3$, $S_3 \rightarrow S_0$, and $S_0 \rightarrow S_1$ transitions fall into the following four categories. (a) Proton release from substrate water and/or its intermediates upon S-state transitions. Such transitions including proton release should be thermodynamically inhibited by lowering pH. (b) Acid-induced protonation of the amino acid groups that are strongly coupled to the OEC structure and its reactions and hence are detectable in FTIR difference spectra. Protonation of such groups will block the normal reactions in certain transitions. It is noted that proton release from this type of amino acid groups by S-state transitions (i.e., the protonation status of the group is different between the S states) has not been detected by FTIR measurements during the S-state cycle at least for carboxylic (COOH) groups. (c) Acid-induced protonation of the amino acid groups that are not structurally coupled to the Mn cluster but are involved in the proton-transfer pathways. Because such groups work as proton mediators and hence their initial and final structures of each S-state transition do not change, they cannot be detected in FTIR difference spectra. (d) Proton release from nonspecific amino acid groups, which are not directly involved in the water oxidation mechanism but are affected by changes of the electrostatics or the overall protein conformation coupled to the S-state transitions.

Another factor that should be taken into consideration is inhibition by Ca^{2+} release at acidic pH. However, this mechanism is unlikely for the present FTIR measurements. It is known that Ca^{2+}-depleted PSII preparations in the presence of potassium ion induce an S_2/S_1 FTIR spectrum totally different from the usual spectrum (*35*, *41*). The observation that the S_2/S_1 spectra detected at acidic pH (pH 3.5−6.0) were basically identical to the standard one at pH 6.0 (Figure 1) indicates that the active centers capable of the $S_1 \rightarrow S_2$ transition retain Ca^{2+} in the OEC even at low pH. It should be noted that the PSII core samples were suspended in acidic buffer only for a short time (<1 min) before forming hydration films. Prolonged incubation in acidic buffer could release Ca^{2+} along with disintegration of the Mn cluster.

The reported pH dependence of the flash-induced proton release patterns of the PSII-enriched membranes of spinach

(*61*) and of the PSII core complexes of *T. elongatus* (*62*) was significantly different; in the former preparation, the proton release pattern was 1.0:0.5:1.0:1.5 at pH 8 and 1.75:0:1.0:1.25 at pH 5.5 for the $S_0 \rightarrow S_1 \rightarrow S_2 \rightarrow S_3 \rightarrow S_0$ transitions (*61*), whereas in the latter preparation, the pattern was 1.0:0.0:1.0:2.0 at pH 7 and 1.0:0.8:1.0:1.2 at pH 5.5 for the same transitions (*62*). These differences may originate from pK_a shifts of amino acid groups that are not directly involved in the catalytic reactions. Therefore, the basically identical pH dependence of the probability of S-state transitions between the two materials (Table 1) indicates that the acidic inhibition in the $S_2 \rightarrow S_3$, $S_3 \rightarrow S_0$, and $S_0 \rightarrow S_1$ transitions is not attributed to factor d.

For factor b, carboxylate and imidazole groups interacting with the Mn cluster by ligation or hydrogen bonding are the most likely candidates. It has been suggested in previous FTIR studies that the catalytic reactions in the $S_1 \rightarrow S_2$ and $S_2 \rightarrow S_3$ transitions are reversed in the $S_3 \rightarrow S_0$ and/or $S_0 \rightarrow S_1$ transitions (*34*, *37*). The first- and second-flash spectra, including the typical COO^- regions of 1600−1500 and 1450−1350 cm^{-1}, did not particularly change by lowering pH to the acidic region (pH < 4), where the $S_3 \rightarrow S_0$ and $S_0 \rightarrow S_1$ transitions are blocked, except for broad backgrounds by buffer reactions (Figures 1−4). Therefore, the observed inhibition of the $S_3 \rightarrow S_0$ and $S_0 \rightarrow S_1$ transitions with p*K* values of 4.2−4.7 (Table 1) cannot be attributed to the protonation of carboxylate groups that are strongly coupled to the Mn cluster. Likewise, the $S_2 \rightarrow S_3$ inhibition with a p*K* value of 3.6 should not be caused by the carboxylate groups coupled to the $S_1 \rightarrow S_2$ transitions, which did not exhibit a specific pH dependence to pH 3.5 (Figure 1). On the other hand, the possibility of strongly coupled histidine residues that are related to the acidic inhibition cannot be excluded at the present stage of knowledge, because the behavior of bands around 1100 cm^{-1}, where the C−N stretching band of histidine has been observed (*46*), was obscured by buffer bands and relatively low signal-to-noise ratios because of the absorption of CaF_2 windows (not shown).

On the basis of these considerations, it is concluded that the observed acidic inhibition of the $S_2 \rightarrow S_3$, $S_3 \rightarrow S_0$, and $S_0 \rightarrow S_1$ transitions is attributed primarily to the factor a. Second also, the factor c has to be taken into account. With this respect, Bernát et al. (*28*) previously proposed the involvement of carboxylate groups located in the proton channel. In fact, the recent X-ray structure by Ferreira et al. (*9*) showed that D1-Asp61, D1-Glu65, and D2-Glu312 are located in the hydrophilic pathways between OEC and the lumenal surface. In addition, further analysis of the X-ray structure showed that the proton channel proceeds along a hydrophilic pathway within the PsbO protein involving Asp158, Asp222, Asp223, Asp224, and Glu229 (*63*). Both mechanisms a and c are indicative of the view that proton release takes place in all S-state transitions except for $S_1 \rightarrow S_2$. This conclusion is basically consistent with the conventional view of the proton release pattern, 1:0:1:2, for $S_0 \rightarrow S_1 \rightarrow S_2 \rightarrow S_3 \rightarrow S_0$ transitions (*14*−*17*, *62*).

In contrast to the pH dependence in the acidic region, our data showed that the efficiencies of all four S-state transitions remain generally high in the alkaline region to pH 9.5 in the complexes that still contain an intact OEC (Figures 7 and 8 and Table 1). Only the $S_2 \rightarrow S_3$ transition exhibits a slight decrease at pH values higher than 8, with a p*K* value estimated to be 10.2 ± 1.0 (Table 1). Note that this value was estimated by fitting the data to pH 9.5, and at pH 10.0, the OEC actually became completely inactive (traces i of Figures 1−4). This pH dependence of S-state transitions on the alkaline side was somewhat different from the previous results for PSII-enriched membranes (*28*) and thylakoids of spinach (*29*, *30*). In PSII-enriched membranes, a clear pH block was observed in the $S_3 \rightarrow S_0$ (p$K \sim 8.0$) and the $S_2 \rightarrow S_3$ transition was also inhibited at high pH (p$K \sim 9.4$), while the $S_1 \rightarrow S_2$ and $S_0 \rightarrow S_1$ transitions were pH-independent (Table 1) (*28*). Also, the increase in average misses has been observed in spinach thylakoids in the alkaline region (*29*, *30*). This difference between *T. elongatus* and spinach in the pH dependence in the alkaline region suggests that the transition efficiencies are determined by a mechanism different from that in the acidic region. Such a mechanism should be rather related to the characteristics of the PSII proteins of each species. Bernát et al. (*28*) proposed that a pH-induced decrease in the redox potential of the $Y_Z^{\bullet}/Y_Z$ couple is responsible for the alkaline inhibition in spinach PSII membranes. In the PSII core complexes of *T. elongatus*, the TL peaks by $S_2Q_A^-$, $S_2Q_B^-$, and $S_3Q_B^-$ recombinations were previousely detected at about 15 °C higher temperatures than those in spinach PSII membranes. The potential of the acceptor side seems unchanged, because the so-called A_T band, which putatively arises from the $(Y_Z^{\bullet}His^+)Q_A^-$ recombination, showed an identical temperature (*51*). Hence, it seems likely that the redox potentials of the S states in the OEC of *T. elongatus* are generally lower than those in spinach. In this case, the energy gap between the Mn cluster and Y_Z becomes larger, and hence, the efficiencies of S-state transitions would be less sensitive to the decrease in the redox potential of Y_Z by increasing pH.

ACKNOWLEDGMENT

We thank Professor Gernot Renger for critical reading of the manuscript and valuable comments.

REFERENCES

1. Debus, R. J. (1992) The manganese and calcium ions of photosynthetic oxygen evolution, *Biochim. Biophys. Acta 1102*, 269−352.
2. Britt, R. D. (1996) Oxygen evolution, in *Oxygenic Photosynthesis: The Light Reactions* (Ort, D. R., and Yocum, C. F., Eds.) pp 137−164, Kluwer Academic Publishers, Dordrecht, The Netherlands.
3. Yachandra, V. K., Sauer, K., and Klein, M. P. (1996) Manganese cluster in photosynthesis: Where plants oxidize water to dioxygen, *Chem. Rev. 96*, 2927−2950.
4. Renger, G. (2001) Photosynthetic water oxidation to molecular oxygen: Apparatus and mechanism, *Biochim. Biophys. Acta 1503*, 210−228.
5. Yachandra, V. K., DeRose, V. J., Latimer, M. J., Mukerji, I., Sauer, K., and Klein, M. P. (1993) Where plants make oxygen−A structural model for the photosynthetic oxygen-evolving manganese cluster, *Science 260*, 675−679.
6. Peloquin, J. M., Campbell, K. A., Randall, D. W., Evanchik, M. A., Pecoraro, V. L., Armstrong, W. H., and Britt, R. D. (2000) ^{55}Mn ENDOR of the S_2-state multiline EPR signal of Photosystem II: Implications on the structure of the tetranuclear Mn cluster, *J. Am. Chem. Soc. 122*, 10926−10942.
7. Zouni, A., Witt, H. T., Kern, J., Fromme, P., Krauss, N., Saenger, W., and Orth, P. (2001) Crystal structure of photosystem II from *Synechococcus elongatus* at 3.8 Å resolution, *Nature 409*, 739−743.

8. Kamiya, N., and Shen, J.-R. (2003) Crystal structure of oxygen-evolving photosystem II from *Thermosynechococcus vulcanus* at 3.7 Å resolution, *Proc. Natl. Acad. Sci. U.S.A. 100*, 98−103.
9. Ferreira, K. N., Iverson, T. M., Maghlaoui, K., Barber, J., and Iwata, S. (2004) Architecture of the photosynthetic oxygen-evolving center, *Science 19*, 1831−1838.
10. Debus, R. J. (2001) Amino acid residues that modulate the properties of tyrosine Y_Z and the manganese cluster in the water oxidizing complex of photosystem II, *Biochim. Biophys. Acta 1503*, 164−186.
11. Diner, B. A. (2001) Amino acid residues involved in the coordination and assembly of the manganese cluster of photosystem II. Proton-coupled electron transport of the redox-active tyrosines and its relationship to water oxidation, *Biochim. Biophys. Acta 1503*, 147−163.
12. Joliot, P., Barbieri, G., and Chabaud, R. (1969) Model of the system II photochemical centers, *Photochem. Photobiol. 10*, 309−329.
13. Kok, B., Forbush, B., and McGloin, M. (1970) Cooperation of charges in photosynthetic O_2 evolution-I. A linear four step mechanism, *Photochem. Photobiol. 11*, 457−475.
14. Fowler, C. F. (1977) Proton evolution from photosystem II stoichiometry and mechanistic considerations, *Biochim. Biophys. Acta 462*, 414−421.
15. Saphon, S., and Crofts, A. (1977) Protolytic reactions in photosystem II: A new model for the release of protons accompanying the photooxidation of water, *Z. Naturforsch., C: J. Biosci. 32*, 617−626.
16. Wille, B., and Lavergne, J. (1982) Measurement of proton translocation in thylakoids under flashing light using a spin-labeled amine, *Photobiochem. Photobiophys. 4*, 131−144.
17. Förster, V., and Junge, W. (1985) Stoichiometry and kinetics of proton release upon photosynthetic water oxidation, *Photochem. Photobiol. 41*, 183−190.
18. Haumann, M., and Junge, W. (1996) Protons and charge indicators in oxygen evolution, in *Oxygenic Photosynthesis: The Light Reactions* (Ort, D. R., and Yocum, C. F., Eds.) pp 165−192, Kluwer Academic Publishers, Dordrecht, The Netherlands.
19. Rappaport, F., and Lavergne, J. (2001) Coupling of electron and proton transfer in the photosynthetic water oxidase, *Biochim. Biophys. Acta 1503*, 246−259.
20. Klimov, V. V., Allakhverdiev, S. I., Demeter, S., and Krasnovskii, A. A. (1979) Photoreduction of pheophytin in the photosystem 2 of chloroplasts with respect to the redox potential of the medium, *Dokl. Akad. Nauk. SSSR 249*, 227−230.
21. Rappaport, F., Guergova-Kuras, M., Nixon, P. J., Diner, B. A., and Lavergne, J. (2002) Kinetics and pathways of charge recombination in photosystem II, *Biochemistry 41*, 8518−8527.
22. Metz, J. G., Nixon, P. J., Rögner, M., Brudvig, G. W., and Diner, B. A. (1989) Directed alteration of the D1 polypeptide of photosystem II: Evidence that tyrosine-161 is the redox component, Z, connecting the oxygen-evolving complex to the primary electron donor, P680, *Biochemistry 28*, 6960−6969.
23. Renger, G., Gläser, M., and Buchwald, H. E. (1976) The control of the reduction kinetics in the dark of photooxidized chlorophyll a_{II}^+ by the inner thylakoid proton concentration, *Biochim. Biophys. Acta 461*, 392−402.
24. Schlodder, E., and Meyer, B. (1987) pH dependence of oxygen evolution and reduction kinetics of photooxidized chlorophyll a_{II} (P-680) in Photosystem II particles from *Synechococcus* sp., *Biochim. Biophys. Acta 890*, 23−31.
25. Vass, I., and Styring, S. (1991) pH-Dependent charge equilibria between tyrosine-D and the S states in photosystem II. Estimation of relative midpoint redox potentials, *Biochemistry 30*, 830−839.
26. Damoder, R., and Dismukes, G. C. (1984) pH dependence of the multiline, manganese EPR signal for the "S_2" state in PS II particles: Absence of proton release during the $S_1 \rightarrow S_2$ electron-transfer step of the oxygen evolving system, *FEBS Lett. 174*, 157−161.
27. Vass, I., Koike, H., and Inoue, Y. (1985) High pH effect on S-state turnover in chloroplasts studied by thermoluminescence. Short-time alkaline incubation reversibly inhibits $S_3 \rightarrow S_4$ transition, *Biochim. Biophys. Acta 810*, 302−309.
28. Bernát, G., Morvaridi, F., Feyziyev, Y., and Styring, S. (2002) pH dependence of the four individual transitions in the catalytic S-cycle during photosynthetic oxygen evolution, *Biochemistry 41*, 5830−5843.
29. Messinger, J., and Renger, G. (1994) Analyses of pH-induced modifications of the period four oscillation of flash-induced oxygen evolution reveal distinct structural changes of the photosystem II donor side at characteristic pH values, *Biochemistry 33*, 10896−10905.
30. Christen, G., Seeliger, A., and Renger, G. (1999) $P680^{+\cdot}$ reduction kinetics and redox transition probability of the water oxidizing complex as a function of pH and H/D isotope exchange in spinach thylakoids, *Biochemistry 38*, 6082−6092.
31. Noguchi, T., and Berthomieu, C. (2005) Molecular analysis by vibrational spectroscopy, in *Photosystem II: The Water/Plastoquinone Oxido-Reductase of Photosynthesis* (Wydrzynski, T., and Satoh, K., Eds.) Kluwer Academic Publishers, Dordrecht, The Netherlands, in press.
32. Hillier, W., and Babcock, G. T. (2001) S-state dependent Fourier transform infrared difference spectra for the photosystem II oxygen evolving complex, *Biochemistry 40*, 1503−1509.
33. Noguchi, T., and Sugiura, M. (2001) Flash-induced Fourier transform infrared detection of the structural changes during the S-state cycle of the oxygen-evolving complex in photosystem II, *Biochemistry 40*, 1497−1502.
34. Noguchi, T., and Sugiura, M. (2002) Flash-induced FTIR difference spectra of the water oxidizing complex in moderately hydrated photosystem II core films: Effect of hydration extent on S-state transitions, *Biochemistry 41*, 2322−2330.
35. Noguchi, T., Ono, T., and Inoue, Y. (1995) Direct detection of a carboxylate bridge between Mn and Ca^{2+} in the photosynthetic oxygen-evolving center by means of Fourier transform infrared spectroscopy, *Biochim. Biophys. Acta 1228*, 189−200.
36. Noguchi, T., Ono, T., and Inoue, Y. (1995) A carboxylate ligand interacting with water in the oxygen-evolving center of photosystem II as revealed by Fourier transform infrared spectroscopy, *Biochim. Biophys. Acta 1232*, 59−66.
37. Noguchi, T., and Sugiura, M. (2003) Analysis of flash-induced FTIR difference spectra of the S-state cycle in the photosynthetic water-oxidizing complex by uniform ^{15}N and ^{13}C isotope labeling, *Biochemistry 42*, 6035−6042.
38. Chu, H.-A., Debus, R. J., and Babcock, G. T. (2001) D1-Asp170 is structurally coupled to the oxygen evolving complex in photosystem II as revealed by light-induced Fourier transform infrared difference spectroscopy, *Biochemistry 40*, 2312−2316.
39. Chu, H.-A., Hillier, W., and Debus, R. J. (2004) Evidence that the C-terminus of the D1 polypeptide of photosystem II is ligated to the manganese ion that undergoes oxidation during the $S_1 \rightarrow S_2$ transition: An isotope-edited FTIR study, *Biochemistry 43*, 3152−3166.
40. Kimura, Y., and Ono, T. (2001) Chelator-induced disappearance of carboxylate stretching vibrational modes in S_2/S_1 FTIR spectrum in oxygen-evolving complex of photosystem II, *Biochemistry 40*, 14061−14068.
41. Kimura, Y., Hasegawa, K., and Ono, T. (2002) Characteristic changes of the S_2/S_1 difference FTIR spectrum induced by Ca^{2+} depletion and metal cation substitution in the photosynthetic oxygen-evolving complex, *Biochemistry 41*, 5844−5853.
42. Hasegawa, K., Kimura, Y., and Ono, T. (2002) Chloride cofactor in the photosynthetic oxygen-evolving complex studied by Fourier transform infrared spectroscopy, *Biochemistry 41*, 13839−13850.
43. Kimura, Y., Mizusawa, N., Ishii, A., Yamanari, T., and Ono, T. (2003) Changes of low-frequency vibrational modes induced by universal ^{15}N- and ^{13}C-isotope labeling in S_2/S_1 FTIR difference spectrum of oxygen-evolving complex, *Biochemistry 42*, 13170−13177.
44. Noguchi, T., and Sugiura, M. (2000) Structure of an active water molecule in the water-oxidizing complex of photosystem II as studied by FTIR spectroscopy, *Biochemistry 39*, 10943−10949.
45. Noguchi, T., and Sugiura, M. (2002) FTIR detection of water reactions during the flash-induced S-state cycle of the photosynthetic water-oxidizing complex, *Biochemistry 41*, 15706−15712.
46. Noguchi, T., Inoue, Y., and Tang, X.-S. (1999) Structure of a histidine ligand in the photosynthetic oxygen-evolving complex as studied by light-induced Fourier transform infrared difference spectroscopy, *Biochemistry 38*, 10187−10195.
47. Chu, H.-A., Gardner, M. T., O'Brien, J. P., and Babcock, G. T. (1999) Low-frequency Fourier transform infrared spectroscopy of the oxygen-evolving and quinone acceptor complexes in photosystem II, *Biochemistry 38*, 4533−4541.
48. Chu, H.-A., Gardner, M. T., Hillier, W., and Babcock, G. T. (2000) Low-frequency Fourier transform infrared spectroscopy of the oxygen-evolving complex in photosystem II, *Photosynth. Res. 66*, 57−63.

49. Chu, H.-A., Sackett, H., and Babcock, G. T. (2000) Identification of a Mn−O−Mn cluster vibrational mode of the oxygen-evolving complex in photosystem II by low-frequency FTIR spectroscopy, *Biochemistry 39*, 14371−14376.
50. Chu, H.-A., Hillier, W., Law, N. A., and Babcock, G. T. (2001) Vibrational spectroscopy of the oxygen-evolving complex and of manganese model compounds, *Biochim. Biophys. Acta 1503*, 69−82.
51. Sugiura, M., and Inoue, Y. (1999) Highly purified thermo-stable oxygen-evolving photosystem II core complex from the thermophilic cyanobacterium *Synechococcus elongatus* having His-tagged CP43, *Plant Cell Physiol. 40*, 1219−1231.
52. Hienerwadel, R., and Berthomieu, C. (1995) Bicarbonate binding to the non-heme iron of photosystem II, investigated by Fourier transform infrared difference spectroscopy and ^{13}C-labeled bicarbonate, *Biochemistry 34*, 16288−16297.
53. Noguchi, T., and Inoue, Y. (1995) Identification of Fourier transform infrared signals from the non-heme iron in photosystem II, *J. Biochem. 118*, 9−12.
54. Isgandarova, S., Renger, G., Messinger, J. (2003) Functional differences of photosystem II from *Synechococcus elongatus* and spinach characterized by flash induced oxygen evolution patterns, *Biochemistry 42*, 8929−8938.
55. Remy, A., Niklas, J., Kuhl, H., Kellers, P., Schott, T., Rögner, M., and Gerwert, K. (2004) FTIR spectroscopy shows structural similarities between photosystems II from cyanobacteria and spinach, *Eur. J. Biochem. 271*, 563−567.
56. Berthomieu, C., Nabedryk, E., Mäntele, W., and Breton, J. (1990) Characterization by FTIR spectroscopy of the photoreduction of the primary quinone acceptor Q_A in photosystem II, *FEBS Lett. 269*, 363−367.
57. Hienerwadel, R., Boussac, A., Breton, J., and Berthomieu, C. (1996) Fourier transform infrared difference study of $Tyrosine_D$ oxidation and plastoquinone Q_A reduction in photosystem II, *Biochemistry 35*, 15447−15460.
58. Noguchi, T., Ono, T., and Inoue, Y. (1992) Detection of structural changes upon $S_1 \rightarrow S_2$ transition in the oxygen-evolving manganese cluster in photosystem II by light-induced Fourier transform infrared difference spectroscopy, *Biochemistry 31*, 5953−5956.
59. Noguchi, T., Ono, T., and Inoue, Y. (1993) Temperature dependence of the $S_1 \rightarrow S_2$ transition in the oxygen-evolving complex of photosystem II studied by FT-IR spectroscopy, *Biochim. Biophys. Acta 1143*, 333−336.
60. Zhang, H., Fischer, G., and Wydrzynski, T. (1998) Room-temperature vibrational difference spectrum for $S_2Q_B^-/S_1Q_B$ of photosystem II determined by time-resolved Fourier transform infrared spectroscopy, *Biochemistry 37*, 5511−5517.
61. Rappaport, F., and Lavergne, J. (1991) Proton release during successive oxidation steps of the photosynthetic water oxidation process: Stoichiometries and pH dependence, *Biochemistry 30*, 10004−10012.
62. Schlodder, E., and Witt, H. T. (1999) Stoichiometry of proton release from the catalytic center in photosynthetic water oxidation—Reexamination by a glass electrode study at pH 5.5−7.2, *J. Biol. Chem. 274*, 30387−30392.
63. De Las Rivas, J., and Barber, J. (2004) Analysis of the structure of the PsbO protein and its implications, *Photosynth. Res. 81*, 329−343.

BI0483312